Journal of Applied Electrochemistry **32**: 65–72, 2002.

Inhibition of copper corrosion by several Schiff bases in aerated halide solutions

H. MA[1,2], S. CHEN[2,3]*, L. NIU[2], S. ZHAO[2], S. LI[2] and D. LI[2]
[1]*Key Laboratory for Colloid and Interface Chemistry of State Education Ministry, Shandong University, Jinan, 250100, People's Republic of China*
[2]*Department of Chemistry, Shandong University, Jinan, 250100, People's Republic of China*
[3]*State Key Laboratory for Corrosion and Protection of Metal, Shenyang 110015, People's Republic of China*
*(*author for correspondence, fax: +86 531 8565167, e-mail: shchen@sdu.edu.cn)*

Received 30 May 2000; accepted in revised form 18 September 2001

Key words: copper, electrochemical impedance spectroscopy (EIS), inhibition efficiency, Schiff base, steady-state polarization

Abstract

The inhibitive action of three Schiff bases, *N*,*N*′-*o*-phenylen-bis(3-methoxysalicylidenimine) (V–*o*-Ph–V), *N*,*N*′-*p*-phenylen-bis (3-methoxysalicylidenimine) (V–*p*-Ph–V) and *N*-[(2-hydroxy-3-methoxyphenyl)methylene]-histidine (V-His), on copper corrosion in aerated 0.5 mol dm^{-3} NaCl and NaBr solutions was investigated using EIS and steady-state polarization techniques. The inhibitor effectiveness depended strongly on the geometric structure of the Schiff bases. Among the three kinds of Schiff base used, the inhibition efficiency of V–*o*-Ph–V on copper corrosion was the highest, V–*p*-Ph–V the next and V-His the lowest. The Schiff bases inhibited the cathodic current more significantly than the anodic current. The different influences of V–*o*-Ph–V or V–*p*-Ph–V on the anodic and cathodic reactions led to the appearance of a low frequency capacitive loop in the impedance spectra. The inhibition action of the Schiff bases was due to their adsorption on the copper surface followed by complexation with Cu(I) or Cu(II) ions, forming a blocking barrier to copper corrosion.

1. Introduction

Copper is a widely used metal with extensive industrial application and the study of its corrosion inhibition has attracted much attention. Nitrogen and sulfur-containing organic heterocyclic compounds may act as inhibitors for copper dissolution [1, 2] due to the chelating action of heterocyclic molecules and the formation of a physical blocking barrier on the copper surface [3]. Among them the most often used are benzotriazole [4–8], benzimidazole [9] and tetrazole [10]. Benzotriazole has been proved to be one of the most important inhibitors for copper and copper alloy corrosion over a wide temperature and pH range [4–8, 11]. However, benzotriazole and its derivatives are highly toxic [3, 12] and environmental protection requirements necessitate that the use of benzotriazole and its derivatives will be limited [12].

Chloride and bromide ions are known to significantly promote the aqueous corrosion of copper [5, 6, 13]. Extensive research on the mechanism of anodic copper dissolution in NaCl, NaBr and HCl solutions [6, 14–18] has been conducted and a number of different dissolution mechanisms have been proposed. It is usually accepted that the anodic dissolution of copper is under mixed control by the electrodissolution of Cu and the diffusion of soluble $CuCl_2^-$ species from the outer Helmholtz plane into the bulk solution [19]. The mechanism of copper corrosion in neutral chloride and bromide solutions involves copper dissolution at anodic sites and electrochemical reduction of oxygen dissolved in the solutions at cathodic sites [3].

Recently, we have found that the Schiff bases synthesized from 3-methoxysalicylaldehyde, especially *N*,*N*′-*o*-phenylen-bis(3-methoxysalicylidenimine) (V–*o*-Ph–V), exhibit strong inhibition of copper corrosion in chloride solutions of different pH [20–22]. In addition, they are environmentally friendly. The purpose of this work is to characterize the inhibition effect of the Schiff bases, V–*o*-Ph–V, V–*p*-Ph–V and V-His, whose molecular structures are described in Figure 1, on the dissolution and corrosion of copper in aerated NaCl and NaBr solutions and to further interpret the inhibition mechanism.

2. Experimental details

The copper electrode was made from 99.9% pure copper rods 5.8 mm in diameter. The rod specimen was embedded in an epoxy resin mould and only its cross section was allowed to contact the aggressive solutions. The electrode was ground with emery paper to a 2000 polish surface before each experiment, and then rinsed with triply distilled water and finally with alcohol.

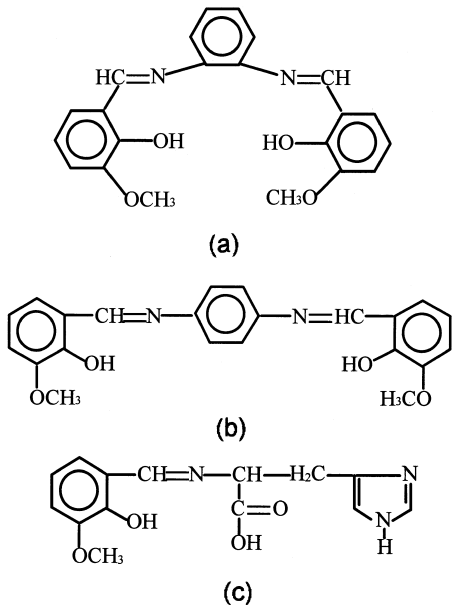

Fig. 1. Structure scheme of several Schiff base molecules: (a) *N*,*N*′-*o*-phenylen-bis(3-methoxysalicylidenimine) (V–*o*-Ph–V); (b) *N*,*N*′-*p*-phenylen-bis(3-methoxysalicylidenimine) (V–*p*-Ph–V); (c) *N*-[(2-hydroxy-3-methoxyphenyl)methylene]-histidine (V-His).

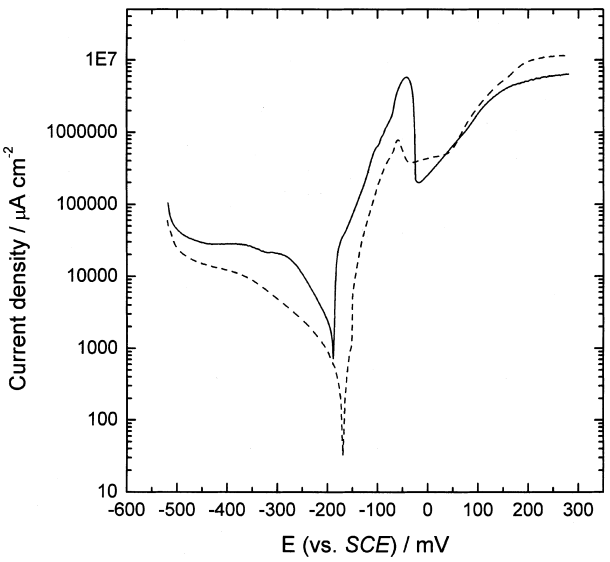

Fig. 2. Steady-state polarization curves for the copper electrode in 0.5 mol dm^{-3} NaCl solutions with and without V–*o*-Ph–V. Key: (——) no V–*o*-Ph–V; (- - -) 1.0×10^{-4} mol dm^{-3} V–*o*-Ph–V, 10 h immersion.

The tests were performed at 20 ± 0.2 °C in a three-electrode cell with a separate compartment for the reference electrode connected with the main compartment via a Luggin capillary. The reference electrode was a saturated calomel electrode (SCE) and the auxiliary electrode was a platinum black electrode with a surface area of 4 cm^2. All potentials are referred to the SCE.

The 2.0 mol dm^{-3} NaCl and NaBr concentrated solutions were prepared with analytical grade NaCl and NaBr reagents and triply distilled water, respectively. The 1.0×10^{-3} mol dm^{-3} V–*o*-Ph–V, V–*p*-Ph–V and V-His were prepared respectively using the synthesized sample and triply distilled water. The 0.5 mol dm^{-3} NaCl or NaBr dilute solutions with and without Schiff bases were prepared through diluting the concentrated NaCl, NaBr and the Schiff base solutions.

Steady-state polarization experiments were conducted with a PAR M273. The polarization curves were obtained by means of the linear potential sweep of 0.2 mV s^{-1} from cathodic to anodic. Impedance measurements were performed with a model 378 a.c. impedance measurement system. Under excitation of a sinusoidal perturbation signal of 5 mV amplitude at the open-circuit corrosion potentials, the frequency was swept from 20 kHz to 10 mHz at five points per decade.

3. Results and discussion

3.1. *Steady-state polarization*

3.1.1. *NaCl solutions with and without V–o-Ph–V*

In the inhibitor-free solution, the anodic polarization curve of copper (solid line in Figure 2) showed a monotonic increase of current with potential until the current reached the maximum at −42 mV vs SCE. A linear region with an apparent Tafel slope of 55 mV $(decade)^{-1}$ was observed above the open-circuit potential (∼−190 mV). This behaviour has been observed by Tromans et al. [5] and Lee et al. [14] and analysed by Bacarella and Griess [19]. The anodic copper dissolution was not solely activation-controlled, but was under mixed control by the electrodissolution of Cu and the diffusion of soluble $CuCl_2^-$ species from the outer Helmholtz plane into the bulk solution [19]. This kind of mixed control resulted in an apparent Tafel slope of 2.303 RT/F, about 60 mV $(decade)^{-1}$. From −42 to −20 mV, the current density declined rapidly with potential increase, forming an anodic current peak centering at −42 mV which was related to CuCl film formation arising from the lateral growth and thickening of CuCl nuclei [5, 6, 13]. In fact, Cu_2O was formed and involved in the formation of CuCl film in neutral aerated NaCl solution. Cu_2O had corrosion protection properties and influenced the electrochemical processes at the copper electrode [11]. At anodic potentials greater than −16 mV, the current increased again with potential.

The cathodic polarization curve displayed a current plateau from −280 to −440 mV. The oxidants in NaCl electrolyte are hydrogen ions and dissolved oxygen. Thermodynamic considerations show that the open-circuit potential (−190 mV) of copper in NaCl solution is much more positive than that of hydrogen evolution (∼−660 mV vs SCE), while dissolved oxygen can be reduced cathodically in the potential region between −280 and −440 mV. In this case, neglect of the hydrogen evolution reaction is a good approximation near the corrosion potential in the presence of oxygen. The cathodic plateau may be attributed to the diffusion-controlled reduction of dissolved oxygen based on thermodynamic analysis [5]. If the anodic current direction is assumed to be in the positive direction, the applied

current density for a corroding electrode whose cathodic reduction is controlled partially by oxygen diffusion can be described by the following equation [23]:

$$i = i_{\text{corr}}\left\{\exp\left(\frac{2.303\,\Delta E}{b_a}\right) - \frac{\exp\left(-\frac{2.303\,\Delta E}{b_c}\right)}{1-\frac{i_{\text{corr}}}{i_L}\left[1-\exp\left(-\frac{2.303\,\Delta E}{b_c}\right)\right]}\right\} \quad (1)$$

where i is the applied current density, i_{corr} the corrosion current density, i_L the cathodic limiting diffusion current density, ΔE the difference between the polarized potential, and the corrosion potential (E_{corr}), b_a the Tafel slope of anodic polarization current curve, and b_c the Tafel slope of cathodic polarization current curve. Provided that the cathodic reduction reaction is determined completely by concentration polarization, namely, $i_{\text{corr}} = i_L$, Equation 1 reduces to

$$i = i_{\text{corr}}\left[\exp\left(\frac{2.303\,\Delta E}{b_a}\right) - 1\right] \quad (2)$$

Consequently, the corrosion potential and the corrosion current of copper in the aerated chloride solutions cannot be determined by the usual Tafel extrapolation method.

In the presence of V–*o*-Ph–V, both the cathodic and anodic current densities were greatly decreased over a wide potential range between −510 and −35 mV, but the V–*o*-Ph–V slightly affected the open-circuit potential (dashed line in Figure 2). It was found from Figure 2 that V–*o*-Ph–V had a much greater influence on the cathodic current than on the anodic one. With increasing positive potential, V–*o*-Ph–V lost anodic inhibition at −27 mV and even began to promote anodic dissolution at more positive potentials. In addition, a current plateau, located in the potential region from −30 to 43 mV, was observed from the curve, which might be ascribed to the occurrence of a weakly passivating film composed of CuCl, Cu_2O and the Cu(I) complex with V–*o*-Ph–V.

We investigated the electrochemical behaviour of copper in NaCl solutions with V–*o*-Ph–V using a PAR M173 potentiostat and a model 368 a.c. impedance measurement system [20, 22]. Some results require verification and some tentative conclusions remain to be confirmed due to the limitation of precision of the instruments. This is the reason for the continuation of the investigation of the electrochemical behaviour of copper in NaCl solutions with and without V–*o*-Ph–V. The results are basically in agreement with previous results, thereby supporting previous conclusions. The purpose of choosing a relatively wide potential region is to investigate how V–*o*-Ph–V affects the anodic and cathodic behaviour of copper. We conclude from Figure 2 that V–*o*-Ph–V is a mixed-type inhibitor of the copper corrosion, but it affects the cathodic reaction rate more significantly.

3.1.2. *NaBr solutions with and without V–o-Ph–V*

The polarization behaviour of copper in the 0.5 mol dm^{-3} inhibitor-free NaBr solution, as indicated by the solid line in Figure 3, was similar to that of copper in the inhibitor-free NaCl solution of the same concentration. The anodic polarization curve also presented an apparent Tafel region with a slope about 57 mV $(decade)^{-1}$ from −250 to −150 mV, an anodic current peak centering at −116 mV, which was associated with the formation of Cu_2O and CuBr mixed film [6], and a wide current plateau starting from about −90 mV caused by a passivating CuBr salt film. The cathodic behaviour was also influenced by the diffusion of oxygen dissolved in NaBr solution, but the effect was not as obvious as in NaCl solution, since the cathodic curve did not show a current plateau.

Under the same conditions, V–*o*-Ph–V affected the polarization behaviour of copper in NaBr solution much more than in NaCl solution. By comparing the dashed lines in Figures 2 and 3, it is seen that when the copper electrode was exposed to the V–*o*-Ph–V-containing halide solutions for 10 h, the anodic and cathodic currents were considerably reduced in NaBr solution. In particular, the large anodic current peak in uninhibited NaBr solution became two small peaks in the V–*o*-Ph–V-containing NaBr solution and the anodic curve no longer exhibited the apparent Tafel region. Although the anodic polarization curve changed more in shape, the cathodic current in NaBr solution was reduced more significantly in the presence of V–*o*-Ph–V.

Figure 3 showed that the shape of the polarization curves depended strongly on the V–*o*-Ph–V concentration and the immersion time. Overall, the higher the V–*o*-Ph–V concentration, the better the inhibition efficiency;

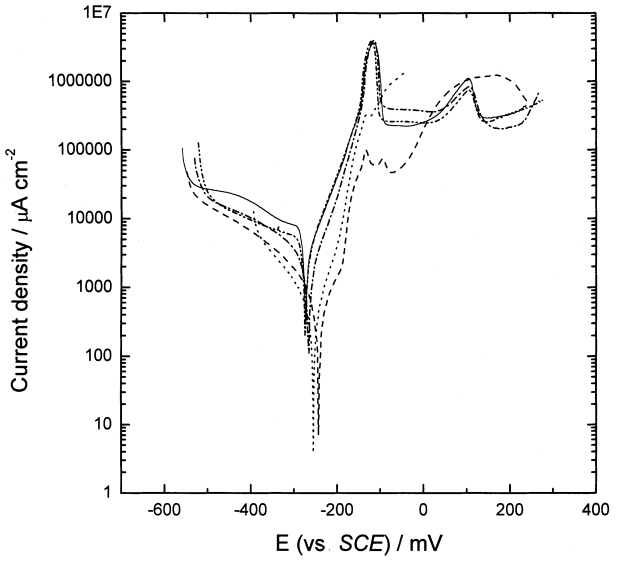

Fig. 3. Comparison of the copper polarization behaviours in 0.5 mol dm^{-3} NaBr solutions with and without V–*o*-Ph–V. Key: (—) no V–*o*-Ph–V; (- - -) 1.0×10^{-4} mol dm^{-3} (10 h immersion); (· · · · · ·) 1.0×10^{-4} mol dm^{-3} (10 min immersion); (-·-·-·) 1.0×10^{-5} mol dm^{-3} (10 h immersion); (- ·····-) 1.0×10^{-5} mol dm^{-3} (1 h immersion).

the longer the immersion time, the better the inhibition efficiency.

V–*o*-Ph–V is a compound with a planar structure (Figure 1(a)) and there are large conjugate π bonds among the three aromatic rings and the two —CH=N— groups. It is inferred that V–*o*-Ph–V adsorbs rapidly on the copper surface and forms a thin protective layer via the formation of a N–Cu coordinate bond or π-electron interactions.

$$\mathrm{Cu} + \text{V–}o\text{-Ph–V} \rightarrow \mathrm{Cu}\text{–}(\text{V–}o\text{-Ph–V})_{\mathrm{ads}} \quad (3)$$

At the same time, complexation of V–*o*-Ph–V with the corrosion products on the copper surface, which exist in the form of Cu_2O or Cu(I) ions, leads to formation of Cu(I)–(V–*o*-Ph–V) chelate.

$$\mathrm{Cu(I)} + \text{V–}o\text{-Ph–V} \rightarrow \mathrm{Cu(I)}\text{–}(\text{V–}o\text{-Ph–V})_{\mathrm{ads}} \quad (4)$$

Inhibition of copper corrosion by V–*o*-Ph–V is probably related to a thin protective film with inclusion of Cu(I)–(V–*o*-Ph–V) chelate compound at the corrosion potential.

When the anodic dissolution of copper begins, Cu(I) ion concentrations around the electrode surface increases; thus V–*o*-Ph–V can form a stable chelate with Cu(I) ions,

$$\mathrm{CuX_2^-} + \text{V–}o\text{-Ph–V} \rightarrow \mathrm{Cu(I)}\text{–}(\text{V–}o\text{-Ph–V})_{\mathrm{ads}} + 2\mathrm{H^+} + 2\mathrm{X^-} \quad (5)$$

It should be noted that Cu(I)–(V–*o*-Ph–V) is unstable and is further oxidized to Cu(II)–(V–*o*-Ph–V) by dissolved oxygen. The Cu(II)–(V–*o*-Ph–V) product was detected on the copper surface in previous work [20]. A crystal of the chelate precipitates on the surface from the solution, resulting in a highly protective thick film on the copper substrate. As a result, the anodic dissolution of copper is inhibited.

Long immersion and high concentration favoured the inhibition effect of V–*o*-Ph–V on copper corrosion. In fact, V–*o*-Ph–V hardly exhibited any influence on the anodic behaviour of copper (see '-···-' in Figure 3) when the V–*o*-Ph–V concentration was low and the immersion time was short.

3.1.3. *Comparison of the polarization behaviour of copper in NaBr solutions with different Schiff bases*

N,*N*′-*p*-phenylen-bis(3-methoxysalicylidenimine) (V–*p*-Ph–V), like V–*o*-Ph–V, is also a planar compound with a big conjugate π bond (Figure 1(b)). The difference in structure between V–*o*-Ph–V and V–*p*-Ph–V is that two —C=N— groups of V–*p*-Ph–V are situated on the opposite of the middle benzene ring. *N*-[(2-hydroxy-3-methoxyphenyl)methylene]-histidine (V-His) is a nonplanar-structure compound (Figure 1(c)). Naturally, no big conjugate π bond can be formed. Figure 4 shows polarization curves of copper in the inhibitor-free NaBr solution and in the presence of three Schiff bases. These

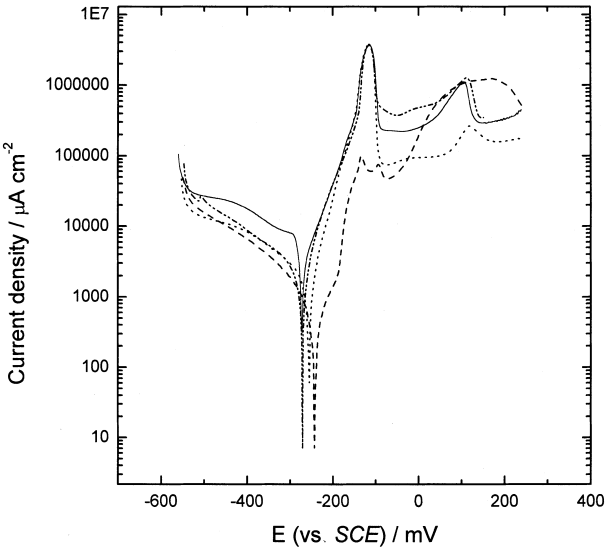

Fig. 4. Steady-state polarization curves for the copper electrode in 0.5 mol dm^{-3} NaBr with and without Schiff bases. Key: (—) no Schiff bases; (-·····-) 1.0×10^{-4} mol dm^{-3} V-His (10 h immersion); (- - -) 1.0×10^{-4} mol dm^{-3} V–*o*-Ph–V (10 h immersion); (·····) 1.0×10^{-4} mol dm^{-3} V–*o*-Ph–V (10 h immersion).

Schiff bases exhibit cathodic inhibition in varying degrees, but V–*p*-Ph–V and V-His have a small influence on the anodic behaviour of copper.

For V–*o*-Ph–V and V–*p*-Ph–V, not only can π electrons enter unoccupied orbitals of copper, but the π^* orbital can also accept electrons of the d orbitals of copper to form feedback bonds [21, 22]. Thus, more than one center of chemical adsorption action may form [21]. Therefore, the inhibition efficiency of V–*o*-Ph–V or V–*p*-Ph–V on anodic dissolution or corrosion of copper should be much higher than that of V-His.

The three Schiff bases can form chelates with Cu(I) or Cu(II) ions. Figure 5(a) shows that one V–*o*-Ph–V molecule may form a stable chelate with Cu(II) ions, whereas this case is not suitable for V–*p*-Ph–V and V-His. The molecular structure of V–*p*-Ph–V means that the two coordinating N atoms cannot form a stable pentaatomic or hexaatomic ring with Cu(II) ion as V–*o*-Ph–V does; the most effective path is that two V–*p*-Ph–V molecules simultaneously participate in coordination with two Cu(II) ions, forming the stable complex shown in Figure 5(b). The same applies to the coordination of V-His with the Cu(II) ion (see Figure 5(c)). It is obvious that the two chelates described in Figures 5(b) and (c) are not so compact as the one shown in Figure 5(a). Especially, the complex shown in Figure 5(c) has a nonplanar structure. In this case, the inhibition efficiency of V–*o*-Ph–V is the highest, followed by V–*p*-Ph–V and V-His. The steady-state polarization and EIS measurements confirm this.

3.2. *Electrochemical impedance spectroscopy (EIS)*

The Nyquist impedance diagram for copper in uninhibited NaCl solution at the corrosion potential (see

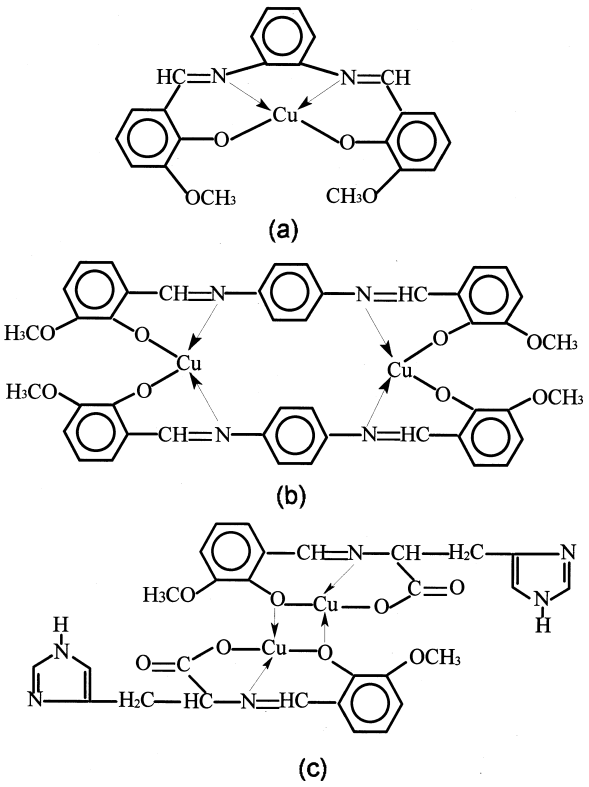

Fig. 5. (a) Structure scheme of Cu(II) chelate with V–*o*-Ph–V; (b) structure scheme of Cu(II) chelate with V–*p*-Ph–V; (c) structure scheme of Cu(II) chelate with V-His.

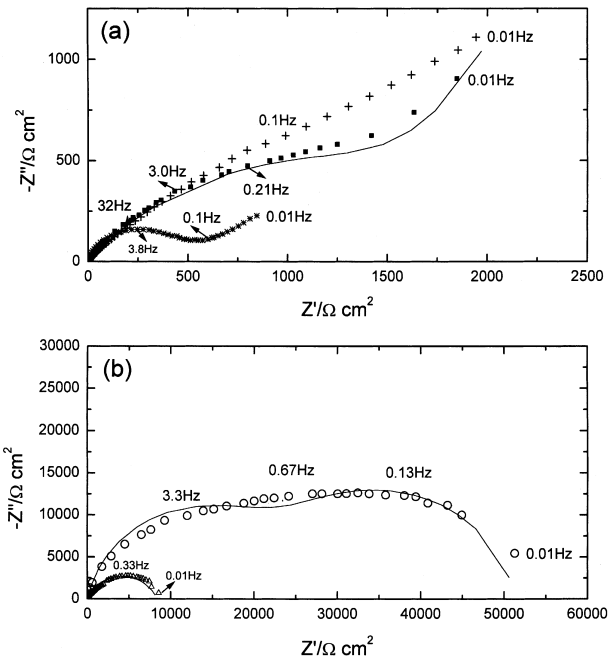

Fig. 6. Nyquist impedance diagrams for a copper electrode in 0.5 mol dm^{-3} NaCl, Na_2SO_4, H_2SO_4 solutions without V–*o*-Ph–V and in 0.5 mol dm^{-3} NaCl solutions with V–*o*-Ph–V at the corrosion potentials. Scatter graphs: measured spectra; line graphs: fitted spectra. Key for upper plot (a): (●) 0.5 mol dm^{-3} NaCl; (+) 0.5 mol dm^{-3} Na_2SO_4; (∗) 0.5 mol dm^{-3} H_2SO_4. Key for lower plot (b): (○) 1.0×10^{-4} mol dm^{-3} V–*o*-Ph–V (10 h immersion); (△) 1.0×10^{-4} mol dm^{-3} V–*o*-Ph–V (10 min immersion).

Figure 6(a)) displayed a Warburg impedance, indicating a diffusion effect. Although the dissolution of copper and the reduction of oxygen take place simultaneously on the electrode surface at the corrosion potential, we believe that the Warburg impedance can be attributed to diffusion of dissolved oxygen from the bulk solution to the electrode surface. This inference is indirectly supported by the fact that the Nyquist diagram for copper measured in dilute H_2SO_4 or Na_2SO_4 at the respective corrosion potentials displays an obvious Warburg impedance. For the Cu/H_2SO_4 (or Cu/Na_2SO_4) system, concentration polarization is believed not to be involved in the anodic dissolution of copper.

The impedance display of copper changed greatly in shape and size when V–*o*-Ph–V was added to NaCl solutions (Figure 6(b)). The Warburg impedance disappeared and the impedance diagrams increased in size. The impedance diagrams for copper in the V–*o*-Ph–V-containing NaCl solutions displayed a depressed capacitive loop in the case of 10 min immersion and two well-separated depressed capacitive loops in the case of 10 h immersion. The same is true of the impedance for copper in NaBr solutions (Figure 7).

At the corrosion potential, the Cu(I) concentration is not high enough to form Cu(I)–(V–*o*-Ph–V) chelate via Equation (4). The inhibition action of V–*o*-Ph–V is probably realized through formation of a Cu–$(V–o\text{-Ph–V})_{ads}$ thin layer via Equation (3). Figures 2 and 3 show that V–*o*-Ph–V has a different influence on the anodic

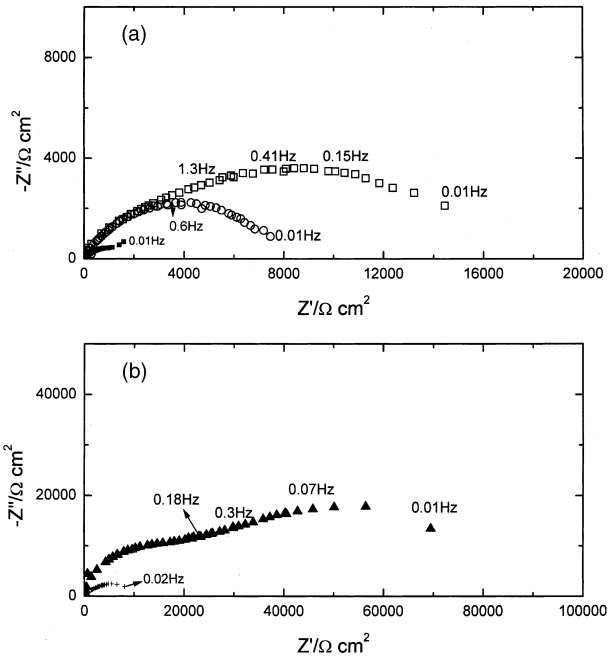

Fig. 7. Nyquist impedance diagrams for the copper measured in the inhibitor-free NaBr solutions and in the NaBr solutions with a different V–*o*-Ph–V concentration at corrosion potentials in the case of different immersion time. Key for upper plot: (a): (●) no V–*o*-Ph–V (□) 1.0×10^{-5} mol dm^{-3} V–*o*-Ph–V (10 h immersion); (○) 1.0×10^{-5} mol dm^{-3} V–*o*-Ph–V (10 min immersion). Key for lower plot (b): (▲) 1.0×10^{-4} mol dm^{-3} V–*o*-Ph–V (10 h immersion); (+) 1.0×10^{-4} mol dm^{-3} V–*o*-Ph–V (10 min immersion).

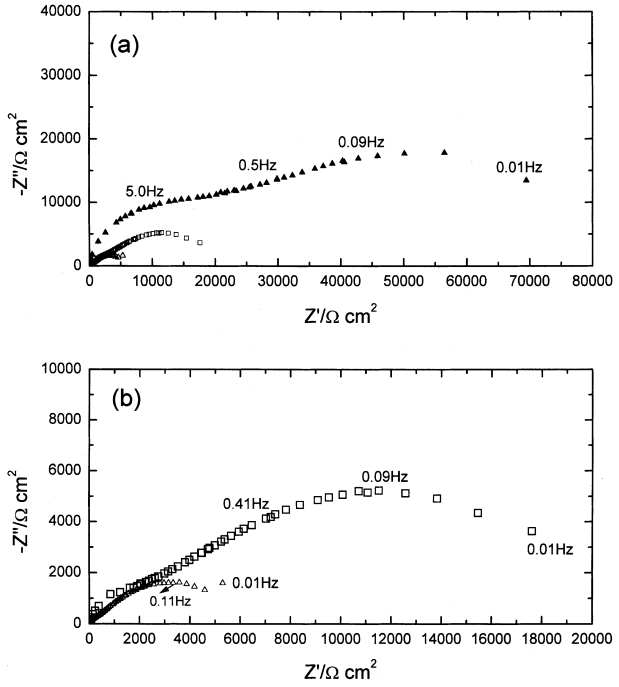

Fig. 8. Nyquist impedance plots for copper measured, respectively, in 0.5 mol dm^{-3} NaBr solutions with V–*o*-Ph–V, V–*p*-Ph–V and V-His at the respective corrosion potentials after the copper electrode was immersed in the solution for 10 h. Key for upper plot (a): (□) 1.0×10^{-4} mol dm^{-3} V–*p*-Ph–V; (△) 1.0×10^{-4} mol dm^{-3} V-His; (▲) 1.0×10^{-4} mol dm^{-3} V–*o*-Ph–V. Key for lower plot (b): (△) 1.0×10^{-4} mol dm^{-3} V-His; (□) 1.0×10^{-4} mol dm^{-3} V–*o*-Ph–V.

and cathodic reactions. The appearance of a low capacitive loop for long immersion times may be ascribed to the different effect of V–*o*-Ph–V on the anodic and cathodic reactions. When the immersion time is short, Cu–$(V–o\text{-Ph–V})_{ads}$ only acts as a blocking layer, inhibiting the anodic and cathodic reactions equally. Accordingly, the impedance plots do not exhibit the low frequency capacitive loop (Figure 8(a)).

The Nyquist spectrum for the copper in the presence of V–*p*-Ph–V also displayed two poorly separated capacitive loops (Figure 8(b)), showing that V–*p*-Ph–V could not inhibit the anodic and cathodic reactions equally on copper for long immersion as V–*o*-Ph–V did. However, the impedance diagram for copper in V-His-containing NaBr solution gave a capacitive loop and a Warburg impedance, which implied that V-His coverage on the copper surface was low and corrosion still proceeded on uncovered sites.

The impedance spectra with Warburg impedance and those displaying one or two capacitive loops may

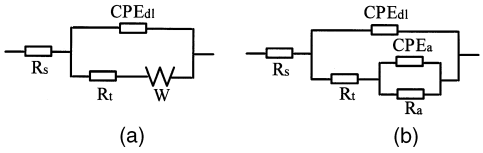

Fig. 9. Equivalent circuit to fit the EIS for copper displaying (a) a Warburg impedance; and (b) one or two capacitive loops.

be analyzed using the electrical circuits shown by Figure 9(a) and (b), respectively. R_s represents the solution resistance, R_t is the charge-transfer resistance, R_a is the pseudo-resistance and W is the Warburg impedance. Constant phase elements (CPEs) are substituted for the capacitive elements to give a more accurate fit. CPE_{dl} represents the double-layer capacitance and CPE_a the pseudo-capacitance. The values of elements of circuits (a) and (b) obtained by fitting the corresponding impedance spectra are given in Tables 1 and 2, respectively. Figure 6(a) shows the fitted impedance spectrum for copper in inhibitor-free NaCl solution, and Figure 6(b) shows the fitted impedance spectra for copper in V–*o*-Ph–V-containing NaCl solutions after immersion for 10 min and 10 h. Moreover, based upon a recently developed impedance analysis [24], the double-layer capacitance and pseudo-capacitance are calculated and the results are listed in Tables 1 and 2.

The high frequency semicircle is generally associated with the relaxation of the electrical double-layer [25, 26]. The diameter of the high-frequency capacitive loop can be considered as the charge-transfer resistance. The smaller the charge-transfer resistance, the faster the corrosion rate. When the corrosion current cannot be determined by the Tafel extrapolation method, the charge-transfer resistance can still be used to evaluate the metal corrosion rate. The inhibition efficiency (ε) can be determined from Eq. (6) [22]:

$$\varepsilon = \left(\frac{R_t - R_t'}{R_t}\right) \times 100 \qquad (6)$$

where R_t is the charge-transfer resistance in the inhibitor-containing halide solutions and R_t' is that in the inhibitor-free solutions. IE values for the Schiff bases on copper are listed in Table 3. V–*o*-Ph–V gave a very high inhibition efficiency, exceeding 90% for copper electrode immersed for 10 h in halide solution of 1.0×10^{-4} mol dm^{-3} V–*o*-Ph–V concentration. But the inhibition efficiency for V–*p*-Ph–V was about 78.9% and for V-His was only 37.1%.

Table 1. Values of the elements of equivalent circuit in Figure 9(a) required for fitting the EIS displaying the Warburg impedance

Solutions	R_t /Ω cm^2	CPE_{dl} Y_0/Ω^{-1} cm^{-2} s^{α}, $\alpha/0 \sim 1$	C_{dl} /μF cm^{-2}	W /Ω cm^2
NaCl	1.21×10^3	7.09×10^{-5}, 0.66	30.9	1.26×10^{-3}
NaBr	1.32×10^3	1.39×10^{-4}, 0.59	43.4	7.46×10^{-4}
0.5 M NaBr + 1.0×10^{-4} M V-His (10 h immersion)	2.10×10^3	8.51×10^{-5}, 0.63	30.6	7.22×10^{-4}

Table 2. Values of the elements of equivalent circuit in Figure 9(b) required for fitting the EIS for copper in NaCl and NaBr solutions with V–*o*-Ph–V, V–*p*-Ph–V

Immersion time	R_t /Ω cm^2	CPE_{dl} Y_0/Ω^{-1} cm^{-2} s$^{\alpha}$, $\alpha/0 \sim 1$	C_{dl} /μF cm^{-2}	R_a /Ω cm^{-2}	CPE_a Y_0/Ω^{-1} cm^{-2} s$^{\alpha}$, $\alpha/0 \sim 1$	C_a /μF cm^{-2}
0.5 M NaCl + 1.0×10^{-4} M V–*o*-Ph–V						
10 min	8.33×10^3	1.92×10^{-5}, 0.73	9.77	–	–	–
10 h	2.63×10^4	1.41×10^{-6}, 0.93	1.10	5.34×10^4	1.57×10^{-5}, 0.47	12.9
0.5 M NaBr + 1.0×10^{-5} M V–*o*-Ph–V						
10 min	7.12×10^3	4.93×10^{-5}, 0.72	32.8	–	–	–
10 h	1.11×10^4	2.17×10^{-5}, 0.73	12.9	–	–	
0.5 M NaBr + 1.0×10^{-4} M V–*o*-Ph–V						
10 min	7.36×10^3	5.09×10^{-5}, 0.67	31.6	–	–	–
10 h	1.46×10^5	1.61×10^{-6}, 0.94	1.25	8.16×10^4	2.65×10^{-5}, 0.49	59.7
0.5 M NaBr + 1.0×10^{-4} M V–*p*-Ph–V						
10 h	6.26×10^3	3.85×10^{-6}, 0.91	2.65	2.10×10^4	7.63×10^{-5}, 0.55	112.1

Table 3. Inhibition efficiency (ε) of three Schiff bases on the copper corrosion under different conditions

Experimental condition	Immersion time	ε/%
0.5 M NaCl + 1.0×10^{-4} M V–*o*-Ph–V	10 min	85.5
0.5 M NaCl + 1.0×10^{-4} M V–*o*-Ph–V	10 h	95.4
0.5 M NaBr + 1.0×10^{-5} M V–*o*-Ph–V	10 min	81.4
0.5 M NaBr + 1.0×10^{-5} M V–*o*-Ph–V	10 h	88.1
0.5 M NaBr + 1.0×10^{-4} M V–*o*-Ph–V	10 min	82.1
0.5 M NaBr + 1.0×10^{-4} M V–*o*-Ph–V	10 h	91.0
0.5 M NaBr + 1.0×10^{-4} M V–*p*-Ph–V	10 h	78.9
0.5 M NaBr + 1.0×10^{-4} M V-His	10 h	37.1

The disappearance of the Warburg impedance shows that the presence of V–*o*-Ph–V or V–*p*-Ph–V in halide solutions changes the mechanism of copper dissolution, or at least may hinder the diffusion of dissolved oxygen to the copper surface. The following two results support this assumption: (i) Table 2 indicates that the double-layer capacitance values changes from 31.1 μF cm^{-2} in NaCl solution to 1.10 μF cm^{-2} in 0.5 mol dm^{-3} NaCl + 1.0×10^{-4} mol dm^{-3} V–*o*-Ph–V solution over 10 h immersion; 37.2 μF cm^{-2} in NaBr solution in the absence of V–*o*-Ph–V to 1.25 μF cm^{-2} in 0.5 mol dm^{-3} NaBr + 1.0×10^{-4} mol dm^{-3} V–*o*-Ph–V over 10 h of immersion. The decrease in double-layer capacitance may be attributed to the fact that the copper surface is covered by V–*o*-Ph–V molecules. Such a small interfacial capacitance suggests no significant corrosion reaction on the copper surface. (ii) The double-layer usually behaves as a constant phase element (CPE) rather than a pure capacitor [24], whose admittance is defined as

$$Y_{CPE} = Y_0(j\omega)^{\alpha} \quad (7)$$

where Y_0 is the magnitude and α is the exponential term [13, 24]. In corrosion studies, the value of α reflects the roughness of the electrode surface. The lower the value of α, the rougher the electrode. From Table 2, α values of the CPE_{dl} are 0.93 in NaCl solution containing 1.0×10^{-4} mol dm^{-3} V–*o*-Ph–V and 0.94 in NaBr solution with 1.0×10^{-4} mol dm^{-3} V–*o*-Ph–V after immersion for 10 h, indicating that copper has hardly been corroded; and the copper surface remains smooth.

The value of pseudo-capacitance is not more than 100 μF cm^{-2} (Table 2), which is much smaller than the pseudo-capacitance caused by the relaxation of adsorbed intermediate species during the metal dissolution. Therefore, the low frequency capacitive loop may be attributed to the different influence of the V–*o*-Ph–V inhibitor on the anodic and cathodic reactions rather than the relaxation of an adsorbed species.

V–*o*-Ph–V inhibits both the anodic and cathodic reactions on the copper surface and can therefore be considered as a kind of mixed type inhibitor in halide solutions. In other words, the inhibition of V–*o*-Ph–V to copper corrosion is not a simple geometric coverage. Otherwise, a Warburg impedance will be observed when the V–*o*-Ph–V partially covers the copper surface and a capacitive loop rather than two capacitive loops can be observed when the V–*o*-Ph–V completely covers the copper surface. The steady-state polarization measurements show that V–*o*-Ph–V affects the cathodic current more strongly than the anodic current. Also, the occurrence of a low frequency capacitive loop further confirms that V–*o*-Ph–V has a greater influence on the cathodic reaction than on the anodic reaction at the corrosion potential. This conclusion also applies to the inhibition of V–*p*-Ph–V on copper.

4. Summary

1. V–*o*-Ph–V and V–*p*-Ph–V behave as mixed-type inhibitors for copper in halide solutions. They decrease the cathodic reaction rate more strongly than the anodic reaction rate, but have little influence on the open-circuit potential of copper in either NaCl or NaBr solutions. The different influences of two Schiff bases on the anodic and cathodic reactions cause the Nyquist diagrams for the copper at the corrosion potential to display a low frequency capacitive loop.
2. The three Schiff bases easily adsorb on the copper surface at the corrosion potentials and form a thin protective film, preventing copper from corrosion.

3. V–*o*-Ph–V inhibits copper corrosion and anodic dissolution more strongly than V–*p*-Ph–V and V-His, since its geometric structure is favourable for forming Cu(II) chelate.

Acknowledgements

This project was supported by Special Funds for the Major State Basic Research Projects G 19990650 and the Chinese National Science Fund 29 873 028 and the Visiting Scholar Foundation of Key Laboratory in Shandong University.

References

1. E. Geler and D.S. Azambuja, *Corros. Sci.* **42** (2000) 631.
2. I. Popova and J.T. Yates Jr, *Langmuir* **13** (1997) 6169.
3. G.P. Cicilo, B.M. Rosales, F.E. Varela and J.R. Vilche, *Corros. Sci.* **41** (1999) 1359.
4. G. Quartarone, G. Moretti, T. Bellomi, G. Capobianco and A. Zingales, *Corrosion* **54** (1998) 606.
5. D. Tromans and R-H. Sun, *J. Electrochem. Soc.* **138** (1991) 3235.
6. T. Aben and D. Tromans, *J. Electrochem. Soc.* **142** (1995) 398.
7. A.K.P. Chu, A.J. Sukawa, *J. Electrochem. Soc.* **116** (1969) 1188.
8. R. Walker, *Corrosion* **31** (1975) 97.
9. G. Lewis, *Corros. Sci.* **22** (1982) 579.
10. F. Zucchi, G. Trabanelli and M. Fonsati, *Corros. Sci.* **38** (1996) 2019.
11. N. Huynh, S.E. Bottle, T. Notoya and D.P. Schweinsberg, *Corros. Sci.* **42** (2000) 259.
12. E. S-Lisac, N. Galic and R. Gasparac, *Corrosion* **56** (2000) 1105.
13. A.V. Benedetti, P.T.A. Sumodjo, K. Nobe, P.L. Cabot and W.G. Proud, *Electrochim. Acta* **40** (1995) 3657.
14. H.P. Lee and K. Nobe, *J. Electrochem. Soc.* **133** (1986) 2035.
15. O.E. Barcia, O.R. Mattos, N. Pebere and B. Tribollet, *J. Electrochem. Soc.* **140** (1993) 2825.
16. J.P. Diard, J.M.L. Canut, B.L. Gorrec and C. Montella, *Electrochim. Acta* **43** (1998) 2485.
17. H.P. Lee, K. Nobe and A.J. Pearlstein, *J. Electrochem. Soc.* **132** (1985) 1031.
18. W.H. Smyrl, *J. Electrochem. Soc.* **132** (1985) 1556.
19. A.L. Bacarella and J.C. Griess Jr, *J. Electrochem. Soc.* **120** (1973) 459.
20. S-L. Li, H-Y. Ma, S-B. Lei, R. Yu, S-H. Chen and D-X. Liu, *Corrosion* **54** (1998) 947.
21. S-L. Li, S-H. Chen, S-B. Lei, H-Y. Ma, R. Yu and D-X. Liu, *Corros. Sci.* **41** (1999) 1273.
22. S-L. Li, Y-G. Wang, S-H. Chen, R. Yu, S-B. Lei, H-Y. Ma and D-X. Liu, *Corros. Sci.* **41** (1999) 1769.
23. M. Stern, *Corrosion* **14** (1958) 440t.
24. X-J. Wu, H-Y. Ma, S-H. Chen, Z-Y. Xu and A-F. Sui, *J. Electrochem. Soc.* **146** (1999) 1847.
25. O.E. Barcia, O.R. Matoos, N. Pebere and B. Tribollet, *J. Electrochem. Soc.* **140** (1993) 2825.
26. O.E. Barcia and O.R. Matoos, *Electrochim. Acta* **35** (1990) 1601.